Research Square

Preprints are preliminary reports that have not undergone peer review.
They should not be considered conclusive, used to inform clinical practice,
or referenced by the media as validated information.

Effect of Low-Pressure Environments on the Joining Mechanism and process of electromagnetic pulse welding

Gongcheng Peng
Hunan University
Ao Chen
Wurong Huang
Wentao Dai
Guangyao Li
Junjia Cui
Hao Jiang
Quanxiaoxiao Liu
lqxxwkk@hnu.edu.cn

Hunan University https://orcid.org/0009-0001-6609-8237

Research Article

Keywords: Electromagnetic pulse welding, Vacuum environment pressure, Non-destructive testing, S-ALE simulation emulation, Microstructure analysis

Posted Date: November 11th, 2026

DOI: https://doi.org/10.21203/rs.3.rs-10850833/v1

License: This work is licensed under a Creative Commons Attribution 4.0 International License.
Read Full License

Effect of Low-Pressure Environments on the Joining Mechanism and process of electromagnetic pulse welding

Gongcheng Peng[a], Ao Chen[a], Wurong Huang[c], Wentao Dai[c], Guangyao Li[a,b], Junjia Cui[a,b], Hao Jiang[a], Quanxiaoxiao Liu[a,b*]

[a] State Key Laboratory of Advanced Design and Manufacturing Technology for Vehicle, Hunan University, Changsha 410082, China

[b] Shenzhen Automotive Research Institute, Beijing Institute of Technology, Shenzhen 518057, China

[c] SAIC-GM-Wuling Automobile Co., Ltd., Liuzhou 545007, China

Abstract

The in-orbit assembly of space stations and the development of lightweight, multifunctional spacecraft have increased the demand for highly reliable joining technologies for dissimilar materials. Electromagnetic pulse welding (EMPW) is an advanced technology for joining dissimilar metals by high-velocity impact. The welding process and joining mechanism of EMPW plates under different vacuum environment pressures were investigated. The intrinsic correlation between environmental pressure and welding quality was revealed. The results showed that reducing environmental pressure increased the flyer plate velocity and the shear strength of the welded joint, and promoted the formation of complete welds. When the environmental pressure was reduced from 101 kPa to 0.1 kPa, the average peak load of the joint increased by 126%. The internal unwelded width of the weld decreased from 2.04 mm to 1.50 mm, and the weld area increased from 21.92 mm^2 to 35.80 mm^2. Combined with S-ALE numerical simulation and microscopic analysis, it was found that the reduction in environment pressure increased the jet velocity, reduced the interfacial air gap and the interstitial void in the plate, and facilitated the generation of interfacial waveforms and the diffusion of elements. The results demonstrate that environmental pressure plays a critical role in EMPW. It governs interfacial jet

*Corresponding author: Tel.: +86 18933285554; Fax: +86 731 88822051; Email: lqxxwkk@hnu.edu.cn

formation, weld bead development, and joint performance. This study provides insights into reliable solid-state joining of dissimilar materials under low-pressure and vacuum environments.

Keywords

Electromagnetic pulse welding; Vacuum environment pressure; Non-destructive testing; S-ALE simulation emulation; Microstructure analysis

1 Introduction

The increasing demand for high-altitude engineering, vacuum equipment manufacturing, and in-orbit manufacturing has expanded welding applications beyond conventional atmospheric environments. Welding processes are now required to operate under low-pressure, vacuum, and near-vacuum conditions [1–3]. The energy coupling, gas escape, stability of the molten pool or interface, and defect formation mechanisms during the welding process are influenced by different atmospheric pressure conditions. The Al/Cu system meets the dual requirements of lightweight substitution and transitional structures for electrical and thermal conductivity and is widely used in engineering applications. However, due to significant differences in physical properties and a tendency to form brittle intermetallic compounds, it serves as a typical challenging material for welding under extreme conditions [3,4].

Al/Cu joining is intrinsically challenging because of the large differences in physical, thermal, and mechanical properties between aluminum and copper. Although Al/Cu joints are widely used in batteries, automobiles, and electrical systems, conventional fusion welding tends to form brittle Al–Cu intermetallic compounds, leading to reduced joint strength and reliability [6,7]. Electromagnetic pulse welding (EMPW) has been proposed as a new solid-phase welding technique for welding dissimilar metals with different properties. Therefore, EMPW has attracted increasing attention for Al/Cu dissimilar metal joining due to its high efficiency, environmental friendliness, and compatibility with automated production [8–15].The Al/Cu welding has conducted relevant research on EMPW technology in recent years. Wang et al. [16] observed the interfacial microstructure of EMPW joints at different discharge voltages and evaluated the tensile properties of the welded joints, which ultimately resulted in well-bonded welds. Sarvari et al. [17] investigated the effect of different welding gaps on joint properties in EMPW. The results showed that a welding gap of 0.7 mm is better for obtaining a metallurgical bond. Pourabbas et al. [18] stated that the impact angle plays a vital role in the thickness of the intermetallic compound layer and the formation of defects at the weld interface, which affects the impact velocity.

The EMPW parameters such as discharge voltage, welding gap, and impact angle have been studied in depth in the past. However, the auxiliary processes of the EMPW process are also important factors affecting welding quality. Deng et al. [19] proposed a new process with a dual-stage coil system for joining aluminum sheets. A background magnetic field is generated to effectively increase the electromagnetic force during the welding process, thereby improving the welding performance. However, the mechanism of different environmental pressures on weld quality has not been systematically investigated. Therefore, the impact of different environments on the quality of Al-Cu EMPW joints and the underlying welding mechanisms deserves further study.

To investigate welding issues in extreme low-pressure environments, such as high-altitude regions and vacuum conditions, ranging from 0.1 kPa to 100 kPa. In this work, the joints of EMPW at different environment pressures are obtained by a self-designed vacuum EMPW plate welding platform. Firstly, the mechanical properties and interaction mechanisms of the welding joints are revealed. Joints morphology and flyer plate dynamic changes are investigated by tensile testing, non-destructive testing (NDT) and Photonic Doppler velocimetry (PDV). Secondly, the welding mechanism was revealed by Microstructure analysis. The microscopic interface structure was studied through S-ALE numerical simulation combined with optical digital microscopy (ODM), scanning electron microscopy (SEM) and energy dispersive spectroscopy (EDS). This provides a theoretical basis for broadening the EMPW window as well as the range of applications.

2 Materials and methods

2.1 Platform design

The EMPW plate welding platform is built to create and maintain different vacuum environment pressures. The test platform consists of four main components: the electromagnetic pulse generation part, the vacuum environment creation part, the vacuum tooling part and the data detection part, as shown in Fig 1. The low-pressure test chamber RDQ-408CL (internal dimensions W 680 × H 800 × D 750 mm, total

power 1.0 kW) was used for the environmental pressure creation part. The equipment provided a pressure-adjustable welding environment with an ultimate vacuum environment pressure of 0.1 kPa. The EMPW workpiece section was shown in Fig 1(a). The structurally simple welding work area was placed in a vacuum environment and the structurally complex energy transfer area was placed in a normal environment. This compartmentalized structural design reduces the risk of ignition ablation. To ensure gas tightness, seals are configured between the fixed plate and the vacuum box, and between the coil and busbar connections. The data acquisition section is shown in Fig 1(b). The PDV probe was used to acquire flyer plate motion velocity and displacement, and the Roche coil was used to acquire coil current and time.

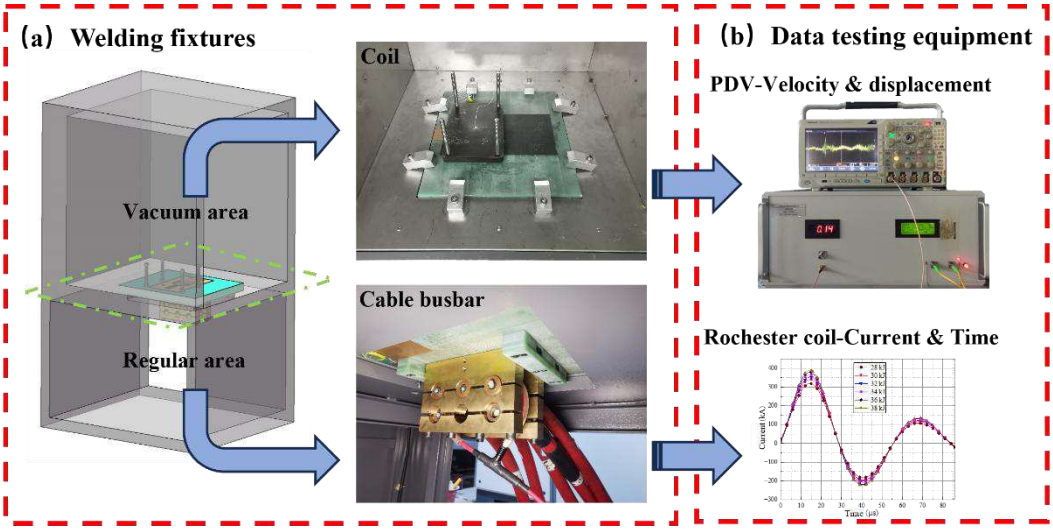


Fig 1 EMPW platform for different environmental pressures: (a) electromagnetic pulse workpiece; (b)data detection part Materials and process

The 1060Al and T2Cu were employed in this study. The mechanical properties and chemical compositions of the two materials were given in Table 1.The experimental principle of connecting the 1060Al and T2Cu plates by EMPW in different environmental pressures. The relative positions and geometries of the Al and Cu plates are shown in Fig 2(a). The dimensions of both plates were 100 mm × 30 mm × 1 mm and the overlap length was 40 mm. To increase environmental involvement in the welding process, the gap between the flyer plate and the base plate was set to 3 mm. The processed material was placed on the tooling and the electromagnetic pulse

generator was discharged through the energy storage after the vacuum tank maintained a preset pressure as shown in Fig 2(b).

Table 1 Mechanical properties and chemical compositions of two materials

Properties	Material	
	1060Al	T2Cu
Density (g/cm3)	2.74	8.96
Poisson's ratio	0.35	0.34
Yield strength (MPa)	40	85
Young modulus (GPa)	68	97
Resistivity (Ω·m)	2.83×10^{-8}	1.678×10^{-8}
Chemical compositions(wt.%)	Cu=0.05, Fe=0.35, Mg=0.03, Mn=0.03, Si=0.25, Ti=0.03, V=0.05, Zn=0.05, Al=balance	Fe=0.005, S=0.005, Ni=0.005, Bi=0.001, Sb=0.002, As=0.002, Pb=0.005 O=0.006, Cu+Ag≥99.9

The current was passed through the cable to the tooling, which generated an alternating magnetic field around the welding coil through the busbar. The flyer plate had high impact velocity with the base plate under the action of the electromagnetic force, thus forming a metallurgical bond between the two metals to be welded, as shown in Fig 2(c.d).

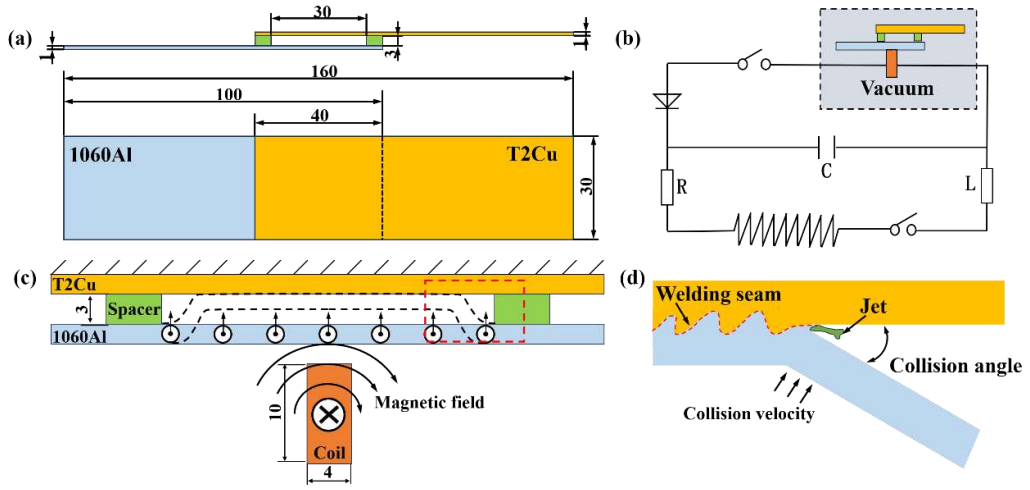


Fig 2 EMPW process of Al-Cu plates in different environment pressures: (a) relative position and geometry of plates; (b) vacuum energy storage and discharge; (c) dynamic response of the flyer plate; (d) metallurgical bonding

In order to select the appropriate discharge energy, discharge energies of 16 kJ, 20 kJ, and 24 kJ were selected for the tests under vacuum environments of 101 kPa and

0.1 kPa. In order to investigate the effects of different environment pressures on the mechanical properties, weld morphology and interfacial structure of EMPW joints in Al-Cu plates. Process tests were carried out under six different environment pressures that could be regarded as equal reductions (101 kPa, 80 kPa, 60 kPa, 40 kPa, 20 kPa, and 0.1 kPa).

2.2 Experimental methods

The flyer-plate velocity was measured using the PDV. The velocity-displacement relationship curves at the velocity measurement points were obtained by processing them through the data processing software. The strength of EMPW joints was evaluated by quasi-static tensile testing using a universal testing machine (LABSANS LD26.105) moving at 2 mm/min. The loads and displacements of the welded joints were collected by a data acquisition system. The weld area and its shape were determined by ultrasonic inspection, and the weld was extracted from the ultrasonic image for measurement. In contrast to the traditional method of stripping the joint and measuring the exposed weld as shown in Fig 3(b). This method was more convenient and accurate, which was especially suitable for samples where there was no fracture in the weld area. Fig 3(c) shows the equipment for ultrasonic NDT. The sample was immersed in water and the probe was located 8.3 mm above the welded sample. The velocity of sound was 4660 mm/s, the sweep length was 60 mm, and the sweep velocity was 20 mm/s.

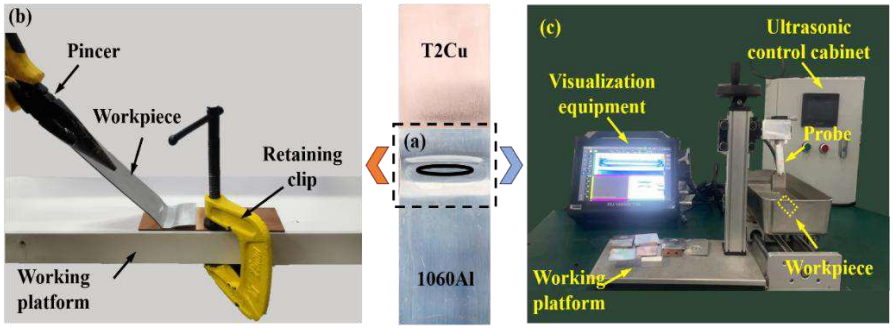


Fig 3 Weld inspection: (a) weld zone; (b) strip tes; (c) ultrasound testing method

Welded specimens with typical mechanical properties were selected and after cutting, mounting and fixing, polishing, they were observed by Olympus ODM, SEM and EDS to further analyse the welded interfaces and evaluate the element distribution.

2.3 Numerical simulation

The structured arbitrary Lagrangian-Eulerian (S-ALE) method has the advantage of capturing fine waveforms and is well suited for applications where the influence of the gaseous medium is not negligible [24]. To further study the EMPW mechanism under different environmental pressures. In this work, a two-dimensional high-velocity oblique collision model of EMPW under different environmental pressures was established based on the S-ALE method using commercial simulation software LS-DYNA. It is used to analyze the microscopic interface deformation behavior of EMPW joints. To obtain the collision velocity and collision angle at the collision point. The collision process of Al and Cu plates under vacuum is simulated by COMSOL in 2D full size as shown in Fig 4.

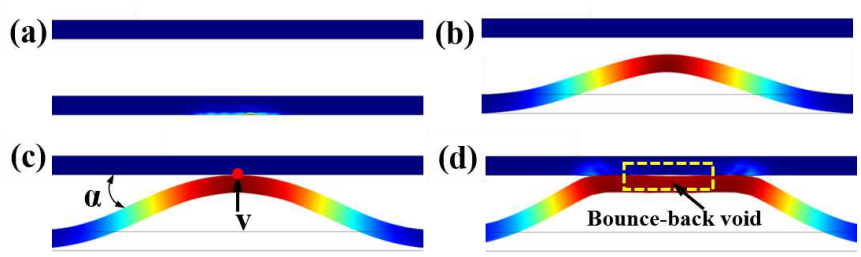


Fig 4 Macroscopic deformation processes of Al and Cu plates colliding:(a) 0 μs；(b) 16.5 μs；(c) 19.1 μs；(d) 21 μs

According to simulation results, the collision velocity v=315 m/s and the collision angle α=14°. The result of the velocity measurement by PDV is 291 m/s, and the difference between the simulation result and the actual one is 8.2%, and the comparison is shown in Fig 5. The accuracy of the numerical simulation results is proved.

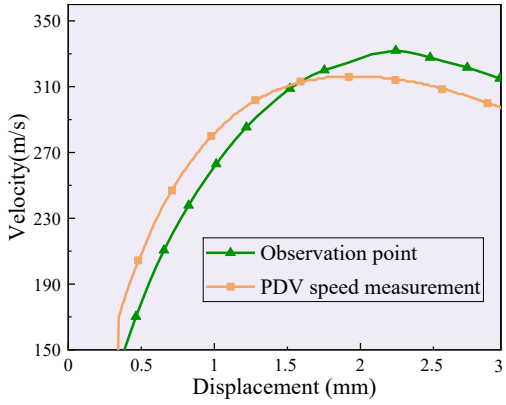


Fig 5 PDV and simulated velocity-displacement curves

Due to the high velocity impact of the two metals during the EMPW process, the Johnson-Cook constitutive model was chosen to describe the material. The constitutive relationship is as follows:

$$\sigma=\left(A+B\varepsilon_p^{\mathrm{n}}\right)\left(1+C\ln\frac{\varepsilon}{\varepsilon_0}\right)\left(1-T^{*m}\right) \tag{1}$$

where σ indicates the yield stress, ε_p is the plastic strain and T^* represents the homologous temperature. A, B, C, n and m are the necessary parameters to define the model. The material parameters used in the simulations were obtained from the research of Liang [25]. In LS-DYNA, the gas density and the actual pressure are the key parameters to describe the gas properties using the empty material model combined with the linear polynomial equation of the gas. The gas parameters at different environmental pressures are shown in Table 2.

Table 2 Air constitutive model and parameters at different environmental pressures

Environment pressures（kPa）	Constitutive model	Air density (kg/m^3)	Air internal energy (J)
101		1.29	0.25×10^6
80		1.022	0.20×10^6
60	*MAT-NULL	0.766	0.15×10^6
40		0.511	0.10×10^6
20		0.255	0.05×10^6
0.1	*MAT-VACUUM	/	/

The geometry and assembly dimensions of the flyer plate and base plate are shown in Fig 6(a). A 0.05 mm square mesh is used to mesh them, as shown in Fig 6(b). The background mesh is generated in LS-Prepost and refined near the collision interface using a 0.005 mm square mesh, as shown in Fig 6(c).

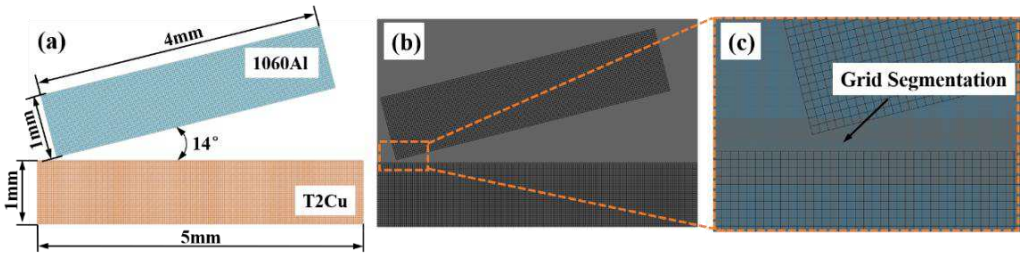


Fig 6 S-ALE simulation modeling process:(a) oblique collision modeling; (b) meshing; (c) background meshing

Finally, the S-ALE simulation results were basically consistent with the microstructural characteristics of the welded joint, as shown in Fig 7, which verified the accuracy of the simulation.

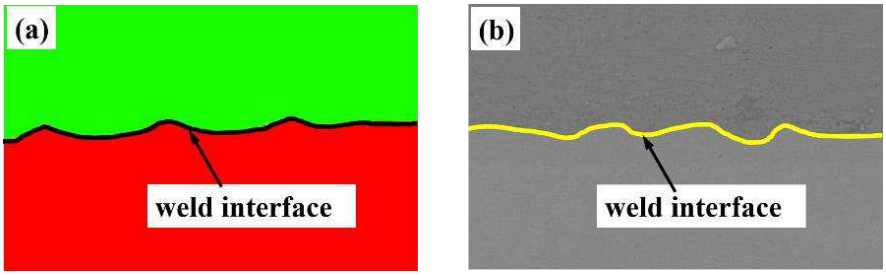


Fig 7 Welding interface comparison image:(a) S-ALE simulation; (b) SEM microscopic observation

3 Results and discussion

3.1 Mechanical properties

3.1.1 Effect of discharge energy

To ensure the appropriate discharge energy, the mechanical properties and failure forms of Al-Cu welded joints under different process parameter combinations were studied through tensile tests. Typical load-displacement curves and failure forms for welded specimens with different process parameters are shown in Fig 8. There were two main types of failure modes: failure located in the weld zone was interface break (IB), and failure was located in the base material tear (BMT).

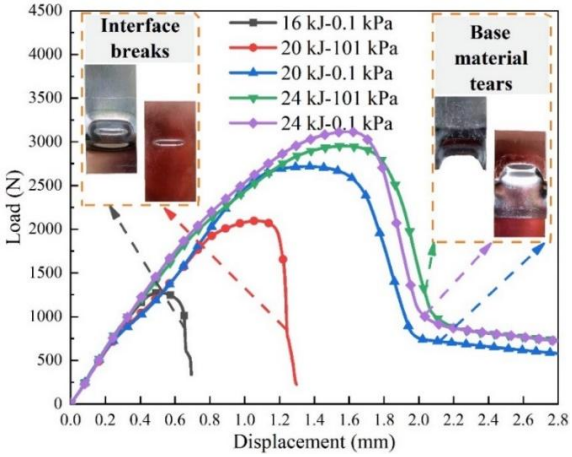


Fig 8 Load-displacement curves and failure forms of welded specimens with different process parameters

Table 3 shows the peak tensile loads and failure forms of repetitive specimens at different energies in vacuum environments of 101 kPa and 0.1 kPa. The peak load increases with rising discharge energy. At the same discharge energy, the peak load is higher at lower-pressure conditions.

At a discharge energy of 16 kJ, the joints were not welded under normal conditions, so no valid data were obtained. At the discharge energy of 20 kJ, the failure forms of the joints changed from IB to BMT, and the average peak load of the joints changed from 2183 N to 2779 N, with a significant improvement in the quality of the weld. At a discharge energy of 24 kJ, the failure forms of the joints were both BMT, and the change in environmental pressure had no significant effect on the mechanical properties of the Al-Cu joints. In order to adequately show the effect of environmental pressure on weld quality, it was desirable to select an energy that would cause significant changes in the mechanical properties of the joint. Therefore, the discharge energy selected in this study to explore the effect of different environmental pressures on the performance of Al-Cu EMPW joints was 20 kJ.

Table 3 Peak tensile loads and failure forms of repetitive specimens

Vacuum environment (kPa)	16 kJ			20 kJ			24 kJ		
	F_{max} (N)	Mean (N)	Failure form	F_{max} (N)	Mean (N)	Failure form	F_{max} (N)	Mean (N)	Failure form
101	/	/	Unwelded	2096 2175 2279	2183	IB	2925 2951 3001	2959	BMT
0.1	1274 1437 1407	1373	IB	2718 2763 2857	2779	BMT	3054 3117 3155	3109	BMT

3.1.2 Effect of vacuum environment

The discharge energy was determined to be 20 kJ, and the load-displacement curves of the specimens in quasi-static tensile tests with different environment pressures are shown in Fig 9(a). The results showed that the carrying capacity of Al-Cu welded joints gradually increased with the decrease of environmental pressure, and the form of failure transitioned from IB to BMT. To investigate the effect of a vacuum environment on the mechanical properties of EMPW joints. Three repetitive tests were conducted on

each type of sample, and the variation of the peak tensile load of the joints with the environmental pressure is recorded in Fig 9(b).

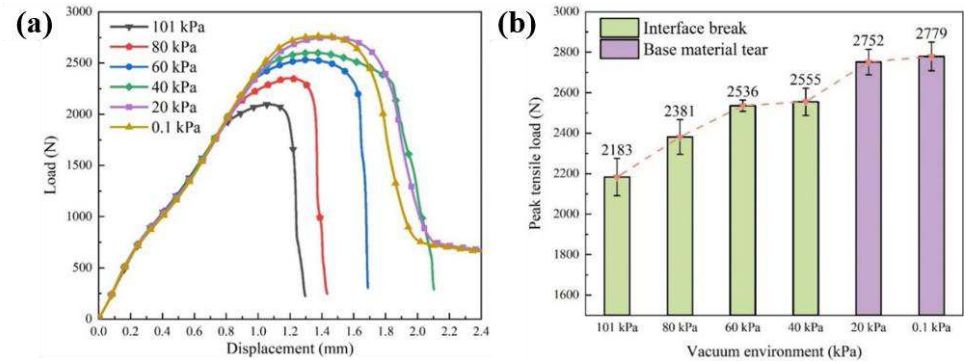


Fig 9 Mechanical properties under different vacuum environment pressures: (a) load-displacement curves; (b) peak tensile loads

The results show an overall increasing trend in the mechanical properties of welded joints as the environment pressure decreases. It can be roughly divided into three parts. When the environment pressure is 101 kPa, 80 kPa and 60 kPa, the failure form of the workpiece is IB. the peak load value of the welded joints increases with the decrease of the environment pressure. Whereas, when the environment pressure is reduced from 60 kPa to 40 kPa, the failure form of workpiece is IB and the peak load remains almost unchanged. When the environment pressure is reduced from 40 kPa to 20 kPa, the failure form of the joint changes and the peak load changes abruptly, and the average peak load of the joint grows from 2555 N to 2752 N. When the environment pressures are 20 kPa and 0.1 kPa, the failure form of the workpiece is BMT, and the average peak load that the joint can withstand is 2752 N and 2779 N, which was about 126% of that at 101 kPa.

To visually investigate the effect of environmental pressure and discharge energy on weld quality, the weld window of the plate at various environment pressures and discharge energies was established at a 3mm gap as shown in Fig 10. The results show that the higher the discharge energy and the lower the environmental pressure, the easier it is to realise the weld and the higher the quality of the weld. However, a higher discharge energy often leads to a reduction in the service life of the equipment and an increase in energy consumption; a lower environmental pressure often leads to time and energy consumption and the generation of the equipment flaming phenomenon.

Therefore, it is necessary to select the appropriate discharge energy and environmental pressure according to the actual situation for different needs and conditions. In this paper, 20 kJ discharge energy and 20 kPa environmental pressure were the optimal combination of parameters. This result provides a reference for the optimisation of EMPW process parameters in actual engineering.

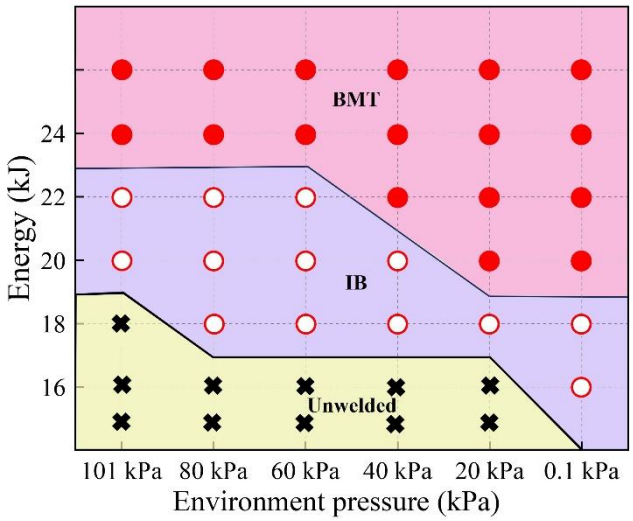


Fig 10 Discharge energy - environment pressure welding window

3.2 The weld morphology of the joints

In order to study the effect of the environment pressure on the weld morphology of the joints, ultrasonic NDT was carried out on the EMPW plate welds obtained under different environment pressures at a fixed discharge energy (20 kJ) and weld gap (3 mm). The morphology of the joints was obtained as shown in Fig 11. Fig 11(b) shows the structural characteristics of a typical weld, which can be divided into four zones: the welds in zones 1 and 3 have a slightly curved quasi-linear morphology, whereas the welds in zones 2 and 4 have an approximately semi-circular profile, which together form a flattened elliptical toroidal weld structure. The weld images of the welded joints at different vacuum environment pressures obtained by the ultrasonic NDT technique are shown in Fig 11(c). The joints at 101 kPa environment pressure showed missing welds in regions 2 and 4, which exhibited the feature of unclosed ends; the joints at 80 kPa environment pressure showed incomplete welds in region 2; and the joints at 60 kPa, 40 kPa, 20 kPa and 0.1 kPa environment pressure all formed a complete annular

weld structure, and the morphological features did not change significantly.

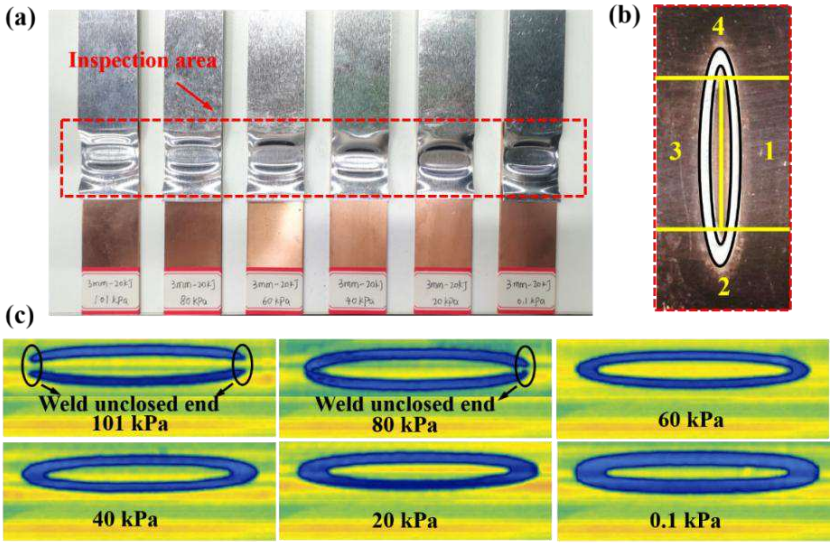


Fig 11 NDT of welds in different environment pressures: (a) inspection area; (b) typical weld morphology; (c) NDT images

Combined with the tensile test data above, the failure forms, peak loads and weld morphology of welded joints at different environment pressures are shown in Table 4.

Table 4 Failure forms, peak loads and weld morphology of welded joints at different environment pressures

Environment pressures (kPa)	Failure forms	F_{max}(N)	Weld morphology
101	IB	2183	double side unclosed
80	IB	2381	single side unclosed
60	IB	2536	full weld
40	IB	2555	full weld
20	BMT	2752	full weld
0.1	BMT	2779	full weld

The table shows that when the environmental pressure is 101 kPa, 80 kPa, 60 kPa and 40 kPa, the failure form of the workpiece is IB. When the environment pressure goes from 101 kPa to 80 kPa, the shape of the joint weld goes from double-sided unclosed to single-sided unclosed, and the peak load is increased by 198 N. The environment pressure goes from 80 kPa to 60 kPa, the shape of the joint weld goes from single side unclosed to full weld, and the peak load is increased by 155 N. This is because joints that have not yet formed a complete weld are subjected to uneven forces during tensile testing, which degrades their mechanical properties. The reduction in

environment pressure can cause the weld morphology to become more complete, improving the mechanical properties of the joint. At 60 kPa, the joint forms a complete circumferential weld. The peak load is almost unchanged when the environment pressure is reduced from 60 kPa to 40 kPa. This is due to the fact that the entire weld morphology is uniformly loaded when tensile tests are performed, so the enhancement effect on the mechanical properties of the joint is small. Subsequently, the failure mode of the workpiece was BMT and the mechanical properties were mainly influenced by the tensile strength of the base metal, independent of the weld morphology. It can be seen that the reduction in environment pressure contributes to weld closure and the formation of a complete circumferential weld. This is a direct result of the improved mechanical properties and the decreasing strengthening effect.

As shown in Fig 12, in order to evaluate the weld morphology, the ultrasonically acquired image of the weld is segmented and extracted. The weld internal width is d (mm), the weld outer width is D (mm), the weld outer length is L (mm), and the weld area is S (mm2). Their positions are shown in Fig 12(a). Three replicate tests were performed on each type of sample.

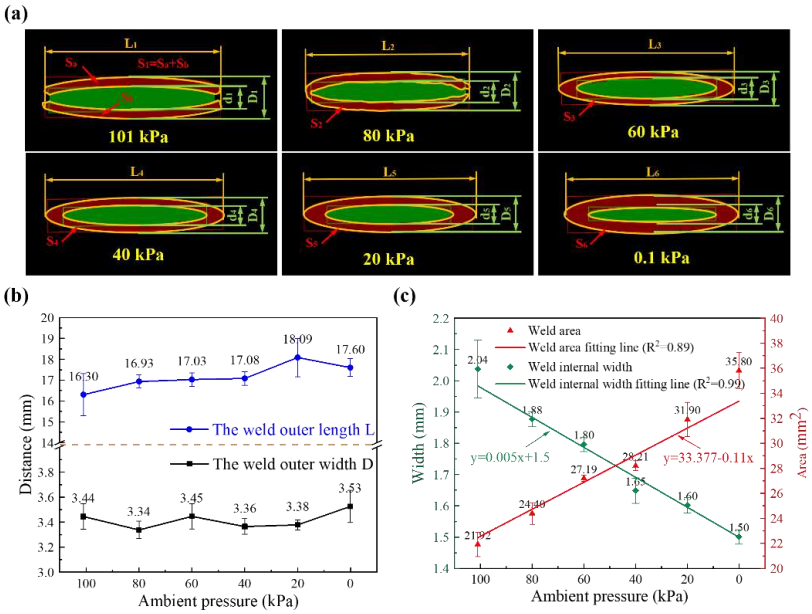


Fig 12 Analysis of weld morphology in different environment pressures: (a) segmentation and extraction of images; (b) weld outer width and weld outer length; (c) weld internal width and weld area

Fig 12(b) records the variation of the weld outer width and weld outer length with

environmental pressure. They were essentially unaffected by environmental pressure. Fig 12(c) records the variation of weld internal width and weld area with environmental pressure and a least squares method is performed to fit a straight line to the sample points. The relationship between the inside width d of the weld and the environment pressure is as follows.

$$y_1 = 0.005x + 1.5 \tag{2}$$

In eq. (2), x is the environment pressure from 101 kPa to 0.1 kPa and y_1 represents the weld internal width. When the environment pressure decreases from 101 kPa to 0.1 kPa, the weld internal width decreases by 26%, from 2.04 mm to 1.50 mm. The relationship between weld area S and environment pressure is as follows.

$$y_2 = 33.377 - 0.11x \tag{3}$$

In eq. (3), x is the environment pressure from 101 kPa to 0.1 kPa and y_2 is the weld area. When the environment pressure decreases from 101 kPa to 0.1 kPa, the weld area increases by 63% from 21.92 mm^2 to 35.80 mm^2. The coefficients of determination for internal weld width d and weld area S are 0.99 and 0.89, respectively, and both explain their correlation with environmental pressure well. This means that as the environment pressure decreases, the internal weld width decreases and the weld area increases. This is also the reason for the change in weld morphology from an unsealed weld to a fully annular weld, as shown in Fig 11. The evolution of the collision velocity and the collision angle can explain this phenomenon. As shown in Fig 13, the distance between the two plates is d. Point O is the initial collision position, and points A and B are the initial and final weld positions, respectively. The distance between point O and point A is half the inside width of the weld d, and the distance between point O and point B is half the outside width of the weld D. The angle formed when the two plates collide is the collision angle α. In general, the greater the collision velocity, the greater the corresponding range of collision angles [12, 26, 27]. Thus, for welded specimens with the same spacing, the inside weld width d decreases with decreasing environment pressure, and point A moves to the left. This may be related to the flyer plate collision velocity.

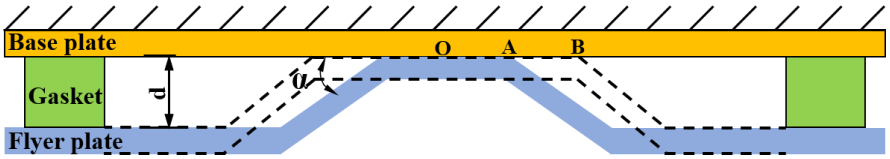


Fig 13 EMPW welding process flyer plate morphology change schematic diagram

3.3 Joining mechanism analysis

In general, the impact velocity of the flyer plate is an important influencing factor in determining the weld morphology and interface structure [28, 29]. In the EMPW process, the density difference between the flyer plate and the air was too large, and the effect of the flyer plate velocity was generally ignored. There was no relevant experimental analysis and demonstration[21]. However, the velocity of the flyer plate was close to the velocity of sound. Air resistance was proportional to the square of the velocity, and a slight change in velocity could make the air resistance increase dramatically. Further, plate welding had a relatively large windward area. There was insufficient justification for ignoring the effect of air resistance based on the density difference alone.

In order to study the effect of environmental pressure on the flyer plate velocity, the discharge energy (20 kJ) and weld gap (3 mm) were fixed, and the flyer plate velocity of EMPW plate welding was measured under normal and vacuum environment pressure. Fig 14 shows the variation curves of the flyer plate velocity with displacement under normal and vacuum environments. The experimental results show that the flyer plate velocity in the initial stage shows an instantaneous increase from 0 m/s to 150 m/s. This phenomenon is attributed to the smaller deformation of the flyer plate in the initial stage and the closer distance between the flyer plate and the coils, which is subjected to a stronger electromagnetic force, resulting in a significant increase in its acceleration. As the displacement increases, the increase in the flyer velocity tends to level off due to the continuous deformation of the flyer resulting in a gradual increase in the distance between the flyer and the coil and the corresponding weakening of the electromagnetic force, resulting in a decrease in the acceleration. When the displacement reaches about 1.5 mm, the flyer plate velocity reaches its peak. After that, the electromagnetic force

is less than the combined force of the deformation resistance of the flyer plate and the air resistance, and the flyer plate enters the deceleration stage. Finally, the flyer plate collides with the baffle plate, causing plastic deformation, and the velocity fluctuates and then rapidly drops to 0 m/s.

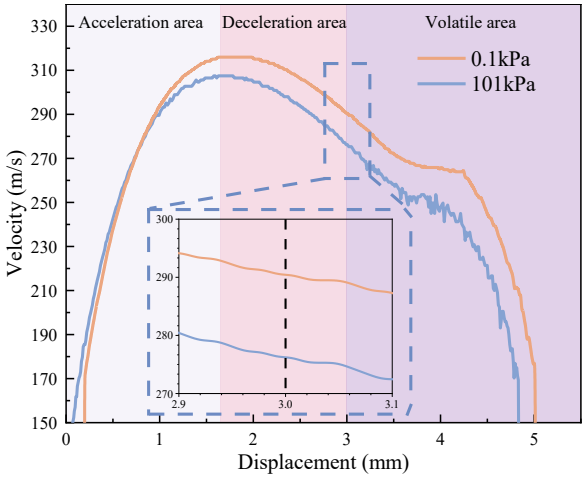


Fig 14 Velocity-displacement curves of flyer plates under different environment pressures

Since the weld gap is 3 mm, the velocity when the flyer plate is displaced to approximately 3 mm is its initial collision velocity. Three repetitive tests were performed for each specimen, and the flyer plate velocities under different environment pressures are shown in Table 5. The results show that when the Al plate collides with the Cu plate, the average velocities of the flyer plates welded in different environmental pressures are 278 m/s and 291 m/s, respectively, under the same discharge energy. It can be seen that the flyer plate velocities increase slightly with the decrease in environmental pressure.

Table 5 Flyer plate velocity at different environmental pressures

Environmental pressures (kPa)	Flyer plate velocity (m/s)	averages (m/s)
101	277	278
	276	
	280	
0.1	290	291
	292	
	291	

The effect of environmental pressure on the microscopic interface during the

contact collision phase is investigated, where different environmental pressure variables are applied after the collision of the flyer plate with the base plate. The environment pressure does not affect the collision velocity and the collision angle after the collision. The collision velocity v = 315 m/s and the collision angle α = 14° are chosen as welding parameters. Fig 15 and Fig 16 show the simulation results of the velocity of the jet and the air between the Al and Cu plates during the EMPW welding process at an environment pressure of 101 kPa and 20 kPa, respectively.

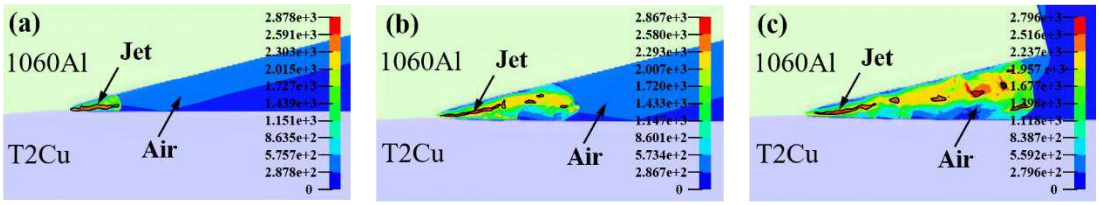


Fig 15 Simulation results of velocity during EMPW process at 101 kPa:

(a)1.5 μs; (b) 3 μs; (c) 4.5 μs

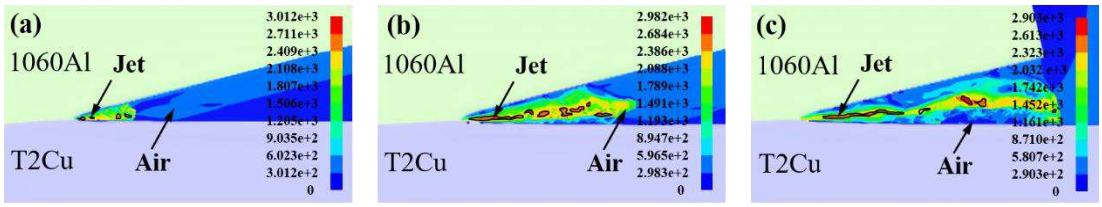


Fig 16 Simulation results of velocity during EMPW process at 20 kPa:

(a)1.5 μs; (b) 3 μs; (c) 4.5 μs

From the figures it can be seen that the jet has a higher velocity than the air at both the 101 kPa and 20 kPa environment pressures. As the welding process progresses, the velocity and range of the air flow increase. This phenomenon can be attributed to the injection of the jets, which move the surrounding air. As the weld progresses, an increasing number of jets are injected, resulting in a greater impact on the surrounding air. Furthermore, the comparison of the jet velocities at an environmental pressure of 101 kPa and 20 kPa shows that the highest jet velocities at different moments at 101 kPa are 2878 m/s, 2867 m/s and 2796 m/s, while the highest jet velocities at different moments at 20 kPa are 3012 m/s, 2982 m/s and 2903 m/s. It has been demonstrated that the velocity of the jet is increased by the reduction of environmental pressure to 20 kPa. The reduction in environmental pressure can increase the jet velocity in the EMPW

collision process. This phenomenon can be attributed to the fact that the reduction of environmental pressure can mitigate the effect of air resistance on the jet velocity.

After the welding of the S-ALE simulation is completed, the microscopic material distribution of the interface of Al-Cu welded joints under two environment pressures is shown in Fig 17. The results demonstrate that the Al-Cu welded interface under both environment pressures exhibits a straight state, and no waveform structure is generated. However, there were more gas gaps at the interface when the environment pressure was 101 kPa. This phenomenon may be attributed to the compression of the gas to the edge of the interface or to a specific region by the shock wave generated at the moment of impact, resulting in incomplete gas discharge. Conversely, the decrease in environmental pressure leads to a reduction in gas density, thereby facilitating complete gas discharge.

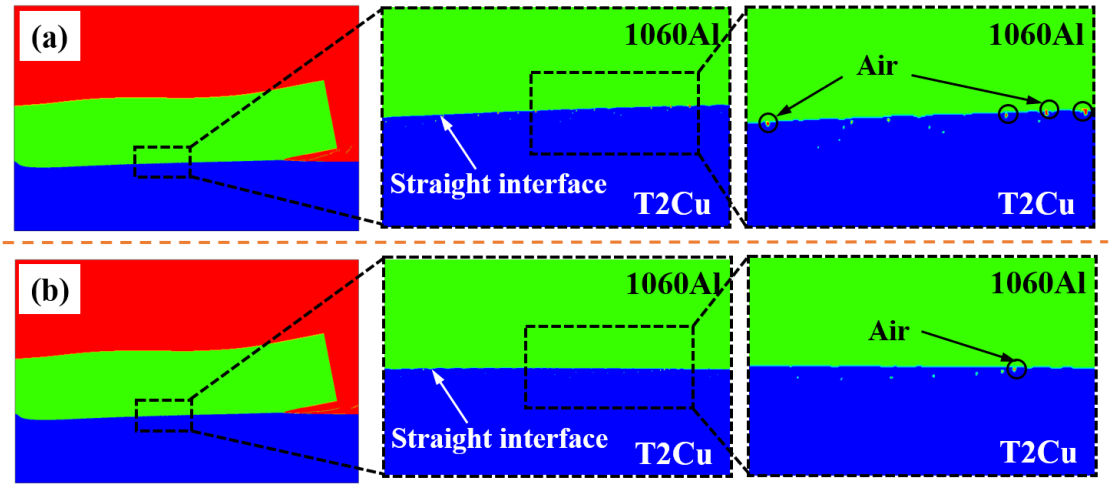


Fig 17 Simulation results of microscopic material distribution at the interface of Al-Cu welded joints under different environment pressures: (a) 101 kPa; (b) 20 kPa

The effect of environment pressure on the microscopic interface is investigated for the full process welding stage, where different environment pressure variables are loaded before the start of the flyer plate movement. It is observed that a decrease in environment pressure results in a modest increase in flyer plate velocity. Through the integration of flyer plate velocity measurements and COMSOL simulations, the collision angle is maintained at 14°, and 315 m/s and 325 m/s are designated as the collision velocity parameters for two-dimensional high-velocity oblique collisions at environmental pressures of 101 kPa and 20 kPa, respectively. Fig 18 and Fig 19 show

the S-ALE simulation results of the Al/Cu welding process under 101 kPa and 20 kPa environment pressure, respectively. The results show that the model successfully simulates the jet phenomenon and the waveform interface occurring during the EMPW welding collision process. A significant metal jet at both 101 kPa and 20 kPa environment pressure, and the color of the jet indicates that the jet material is Al, which is due to the fact that Al plates are significantly weaker than Cu plates and tend to break to form jets during violent collisions. At an environment pressure of 101 kPa, a straight interface is formed; at an environment pressure of 20 kPa, a straight interface is formed at the initial collision stage Fig 19(a)); at 2 μs (Fig 19(b)), a waveform structure appears at the interface; and at 3.8 μs (Fig 19(c,d)), the waveform structure of the interface disappears and the straight interface is restored. Combined with the simulation of the contact collision stage and the simulation of the full process welding stage, it can be seen that the low-pressure environment synergistically promotes the generation of the waveform interface by increasing the flyer plate velocity and the jet velocity.

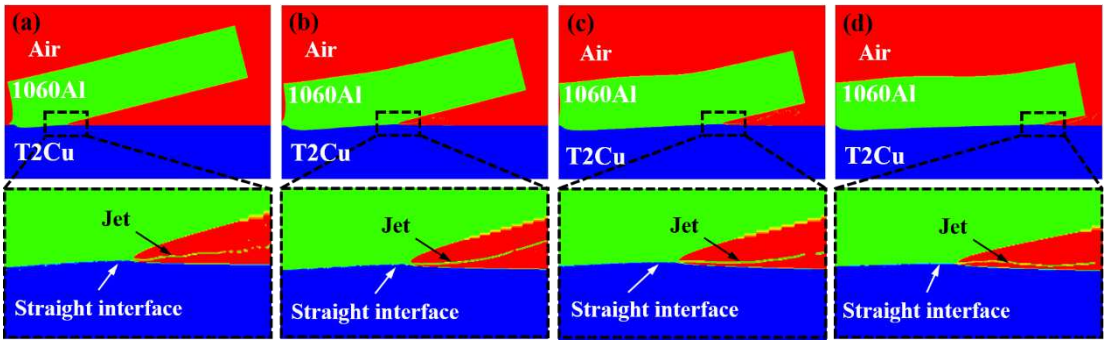


Fig 18 S-ALE simulation results of Al-Cu welding process at 101 kPa:

(a) 1.5 μs; (b) 3 μs; (c) 4.5 μs; (d) 6 μs

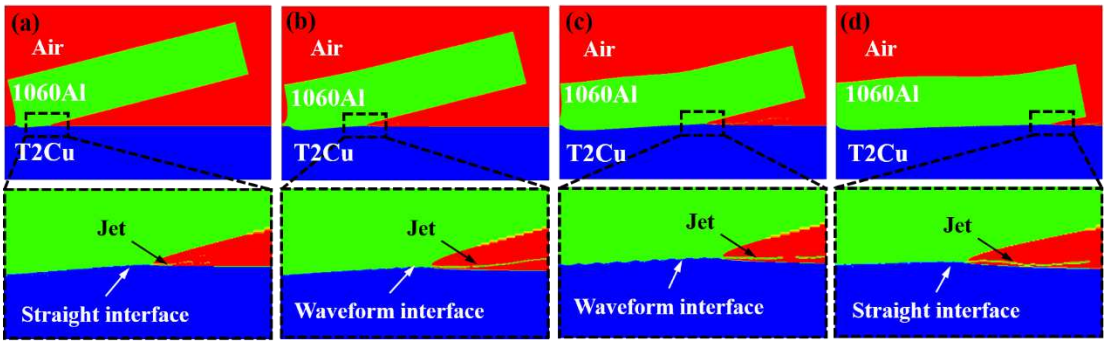


Fig 19 S-ALE simulation results of Al-Cu welding process at 20 kPa:

(a) 1 μs; (b) 2 μs; (c) 3.8 μs; (d) 6 μs

3.4 Microstructure analysis

The weld interface of the EMPW welds at environment pressures of 101 kPa and 20 kPa was observed using an optical digital microscope, and the results are shown in Fig 20.

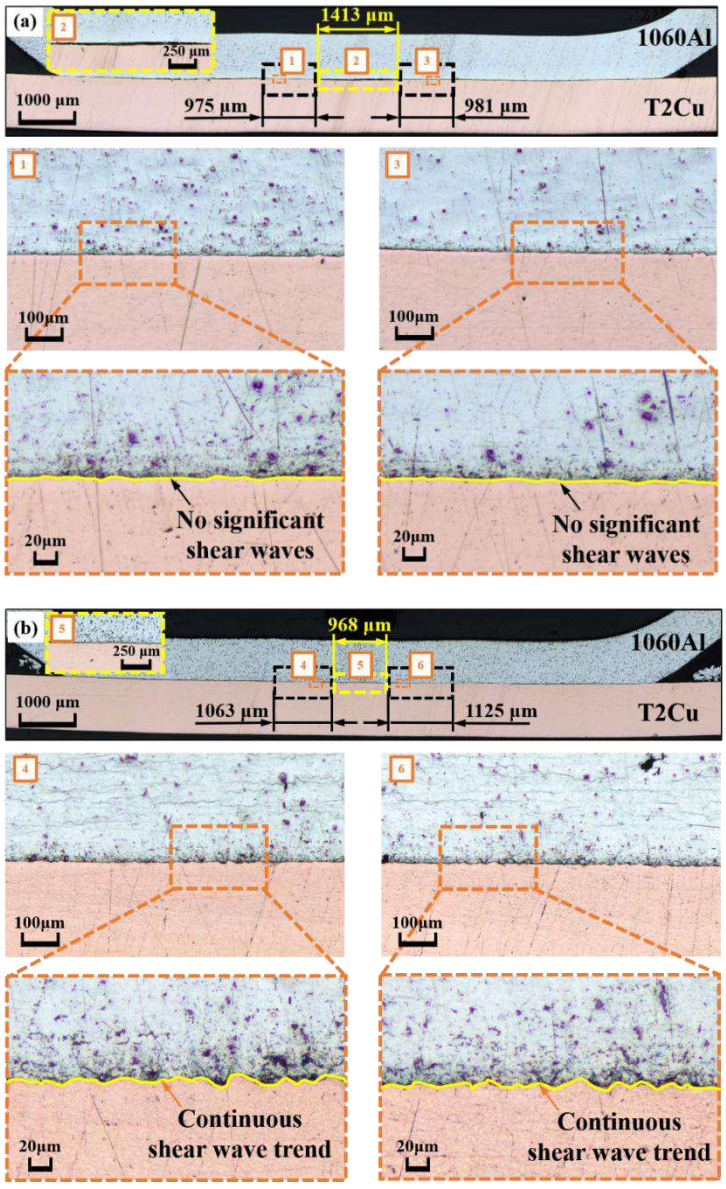


Fig 20 EMPW interface structure in two different environment pressures: (a) 101 kPa environmental pressure; (b) 20 kPa environmental pressure

The evolution of the dynamic behaviour of the flyer plate can explain the above microscopic observations [30]. As shown in Fig 21, the kinematic properties of the flyer plate and the interface forming mechanism during the EMPW process are revealed.

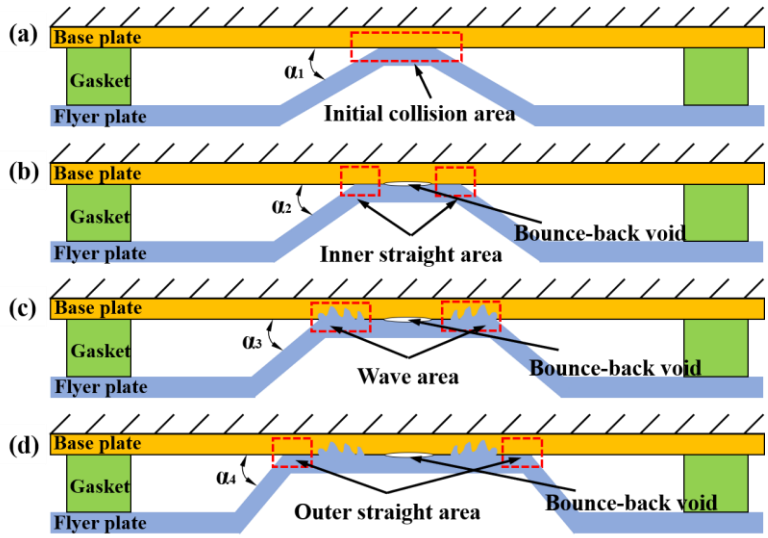


Fig 21 Schematic diagram of the evolution of the dynamic behavior of the flyer plate in EMPW: (a) Stage 1; (b) Stage 2; (c) Stage 3; (d) Stage 4

The interface forming process can be divided into four stages. In the first stage, the initial collision angle of the Al-Cu plate α1 = 0°, the interface bounces back to form a negative displacement, and effective bonding is not achieved in this stage. In the second stage, the collision point moves outward so that the collision angle increases to the critical α2 when the metal jet is triggered, forming a straight welding zone. In the third stage, the collision angle is continuously increased and coupled with the critical velocity condition to realize the interface waveform structure generation. When the collision angle reaches α3, the collision angle increases to the point where the conditions for wave structure formation are no longer met. In the fourth stage, when the change of collision angle and collision velocity destroys the waveform generation condition, the interface returns to straight and terminates the effective bonding.

The weld differences in Fig 20 have been mechanistically analysed by the interface evolution process in Fig 21. In the first stage, there are significant unwelded areas and voids in the centre of the interface of the 101 kPa conventional pressure sample, whereas there are essentially no voids in the interface of the 20 kPa vacuum sample. This is due to the following reasons: when EMPW is performed in a vacuum environment, the centre collision point is caused by a small collision angle, which leads to a high-velocity rebound to form a void, and then the Lorentz forces push the void to be compressed; while the high-velocity deformation of the plate in a conventional

pressure environment leads to the inability to discharge air in a timely manner, and an air cushion is formed in the centre of the interface, which prevents compression and closure. In the second and third stages, the effective weld length of the vacuum specimen is longer than that of the conventional pressure specimen and exhibits the typical waveform interface characteristics. This is due to the fact that the generation of effective welds and the formation of waveform interfaces require sufficient collision and jet velocities. At lower ambient vacuum pressures, the energy loss of the flyer plate and jet can be reduced and the velocity of the flyer plate and jet moving in the air can be increased, thereby promoting the formation of effective welds and the formation of waveform interfaces.

In summary, lower environment pressures reduce or eliminate plate voids at the center of the collision and promote the generation of effective welds and the formation of waveform interfaces, which usually implies better welding results [27, 31].

SEM and EDS were used to characterize the typical weld interface morphology and element distribution of welded joints, and the results are shown in Fig 22 and Fig 23. Typical SEM images of the interface are shown in Fig 22(a) and Fig 23(a). The same results as in Fig 20 can be obtained from the SEM. The welded interface at 101 kPa was relatively flat, while there was an obvious shear wave at the welded interface at 20 kPa. The EDS surface scans illustrated in Fig 22(b) and Fig 23(b) show that Al and Cu have diffused and bonded in the welded interface. Different positions were selected for EDS line scanning, with the test position perpendicular to the waveform interface, which crossed the interface from the Al side to the Cu side. At the weld interface, the area where both Al and Cu elements were present was the elemental diffusion zone. The line scan results at 101 kPa are shown in Fig 22(c,d), which showed elemental diffusion distances of 1.4 μm and 1.6 μm, respectively. The line scan results at 20 kPa are shown in Fig 23(c,d), which showed elemental diffusion distances of 2.2 μm and 2.6 μm, respectively. The weld interface at 20 kPa had a thicker elemental diffusion layer. This might be due to a decrease in environmental pressure, which caused the jet velocity to increase [21]. Thin layers of oxides on metal surfaces were better broken up and removed, revealing a clean metal surface. It would facilitate the

diffusion of elements between the two materials at the weld interface to form a better bonding interface. The reduction in environmental pressure promoted the generation of interfacial waves and the diffusion of elements, which usually meant better welding results[32].

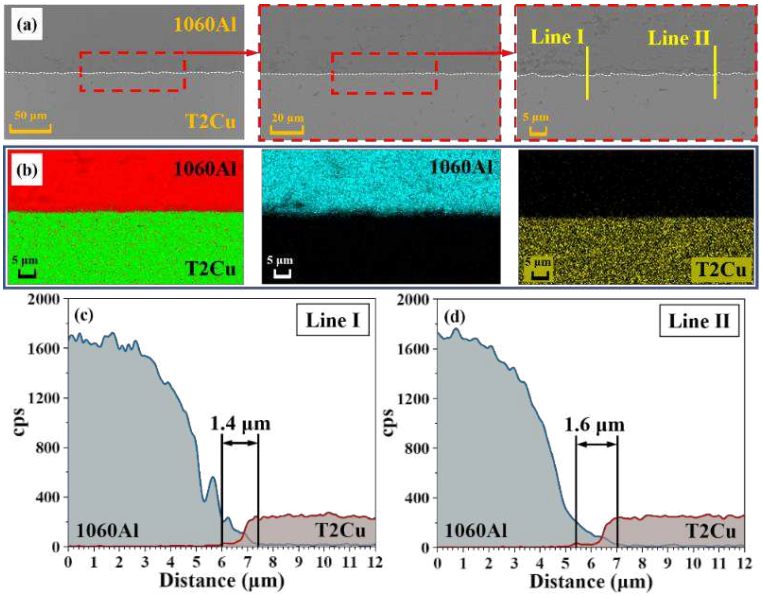


Fig 22 SEM and EDS images of the weld interface at 101 kPa: (a) typical morphology of weld interface; (b) elemental distribution; (c) and (d) show the EDS scans of line 1 and line 2, respectively

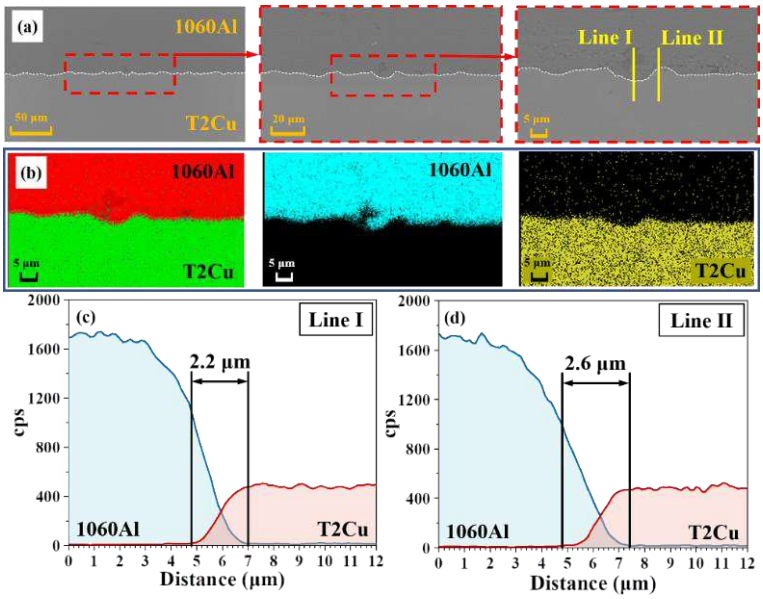


Fig 22 SEM and EDS images of the weld interface at 20 kPa: (a) typical morphology of weld interface; (b) elemental distribution; (c) and (d) show the EDS scans of line 1 and line 2, respectively

4 Conclusion

In this study, the joining mechanism and process of EMPW with 1060Al/T2Cu structures in extreme low-pressure environments pressures are investigated, ranging from 0.1 kPa to 100 kPa. By constructing a vacuum environmental pressure EMPW platform, process tests, numerical simulations, and microscopic interface analysis, the intrinsic connection between environmental pressure and weld quality was revealed. The following main conclusions were drawn from the above study:

(1) The mechanical properties of welded joints formed at different environment pressures were investigated by tensile tests. The results showed that the reduction of environment pressure improved the mechanical properties of the welded joints. When the environment pressure was reduced to 0.1 kPa, the average value of the peak load of the joints was 2779 N, which was about 126.07% of that at 101 kPa. In addition, a window at different environment pressures and discharge energies was established to guide the selection of process parameters.

(2) Ultrasonic NDT was used to evaluate the weld morphology of the plates in different environment pressures. The fitted straight line nicely explained the correlation with environmental pressure. The results showed that decreasing the environmental pressure reduced the weld internal width and increased the weld area. When the environmental pressure was decreased from 101 kPa to 0.1 kPa, the internal width of the weld was reduced by 26% from 2.04 mm to 1.50 mm, and the weld area increased by 63% from 21.92 mm^2 to 35.80 mm^2.

(3) The S-ALE simulation has successfully modeled the jet phenomena and wave interfaces during the EMPW collision process, and it was found that reducing the environment pressure could enhance the jet velocity and reduce the interfacial air gap, which could promote the generation of the waveform interface.

(4) Microscopic observation revealed that the reduction of environment pressure increased the effective weld length, reduced the intermediate unwelded zone length, and basically eliminated the interplate void, which facilitated the generation of interface waveforms and the diffusion of elements. Compared with EMPW under

normal environments, the reduction in environment pressure can reduce the influence of air resistance, increase the flyer plate velocity and jet velocity, and combines with the air cushion effect to change the microscopic interface characteristics. Ultimately, the weld integrity and joint mechanical properties are improved.

Acknowledgements

This project was supported by the National Natural Science Foundation of China (No.52375331) and the Fundamental Research Funds for the Central Universities (No.531118010862).

Conflict of Interest Statement

Conflict of Interest for all authors - None.

Data Availability

The raw/processed data required to reproduce these findings cannot be shared at this time due to technical or time limitations.

References

1. Liu YB, Sun QJ, Wang H, Zhang HM, Cai SJ, Feng JC. Effect of the axial external magnetic field on copper/aluminium arc weld joining. Sci Technol Weld Join. 2016;21(6):460-465. https://doi.org/10.1080/13621718.2015.1125406

2. Rajak AK, Kore SD. Numerical simulation and experimental study on electromagnetic crimping of aluminium terminal to copper wire strands. Electr Power Syst Res. 2018;163:744-753. https://doi.org/10.1016/j.epsr.2017.08.014

3. Lader SK, Baruah M, Ballav R. Significance of underwater friction stir welding on the weld integrity of thin sheets of aluminum (AA1050-O) and brass (CuZn34) joints. Mater Sci Eng A. 2023;865:144974. https://doi.org/10.1016/j.msea.2023.144627

4. Bergmann JP, Petzoldt F, Schürer R, Schneider S. Solid-state welding of aluminum to copper—case studies. Weld World. 2013;57(4):541-550. https://doi.org/10.1007/s40194-013-0049-z

5. Zhao Y, You J, Qin J, Dong C, Liu L, Liu Z, Miao S. Stationary shoulder friction stir welding of Al–Cu dissimilar materials and its mechanism for improving the microstructures and mechanical properties of joint. Mater Sci Eng A. 2022;837. https://doi.org/10.1016/j.msea.2022.142754

6. Mao Y, Qin D, Xiao X, Wang X, Fu L. Achievement of high-strength Al/Cu dissimilar joint during submerged friction stir welding and its regulation mechanism of intermetallic compounds layer. Mater Sci Eng A. 2023;865:144164. https://doi.org/10.1016/j.msea.2022.144164

7. Beygi R, Carbas RJC, Marques EAS, Barbosa AQ, Kasaei MM, da Silva LFM. Mechanism of toughness enhancement of brittle fracture by intermittent η-intermetallic in Al/Cu joint made by FSW. Mater Sci Eng A. 2024;890:145907. https://doi.org/10.1016/j.msea.2023.145907

8. Zhu C, Cui J, Li G, Gao W. Multi-parameters optimization and failure modes investigation of Al/Mg electromagnetic pulse welded joints. Mater Today Commun. 2025;43:111762. https://doi.org/10.1016/j.mtcomm.2025.111762

9. Gavel KS, Ahmed M, Ali A, Bhargaw HN, Panthi SK, Bhargav A. A novel tool design for magnetic pulse welding of sheet metal using compression coil. J Manuf Process. 2025;144:261-277. https://doi.org/10.1016/j.jmapro.2025.02.036

10. Sarvari M, Abdollah-zadeh A, Naffakh-Moosavy H. Investigation of variations of metallurgical and morphological phenomena of interface in the magnetic pulse welding of Al–Cu. J Mater Res Technol. 2025;36:448-458. https://doi.org/10.1016/j.jmrt.2025.03.093

11. Kapil A, Sharma A. Magnetic pulse welding: an efficient and environmentally friendly multi-material joining technique. J Clean Prod. 2015;100:35-58. https://doi.org/10.1016/j.jclepro.2015.03.042

12. Wang S, Zhou B, Zhang X, Sun T, Li G, Cui J. Mechanical properties and interfacial microstructures of magnetic pulse welding joints with aluminum to zinc-coated steel. Mater Sci Eng A. 2020;788:139425. https://doi.org/10.1016/j.msea.2020.139425

13. Deng J, Xie J, Li J, Zhou Y, Wang S, Zhang T, Chen Y. Microstructure and mechanical properties of CoCrFeNiMn HEA/1060Al magnetic pulse welded joints. Mater Charact. 2025;224:115087. https://doi.org/10.1016/j.matchar.2025.115021

14. Ben-Artzy A, Stern A, Frage N, Shribman V, Sadot O. Wave formation mechanism in magnetic pulse welding. Int J Impact Eng. 2010;37(4):397-404. https://doi.org/10.1016/j.ijimpeng.2009.07.008

15. Su Z, Yin L, Jiang H, Zhang L, Chen Y, Zhang L, Zhang H, Feng W. Research progress of electromagnetic pulse welding technology: A review. J Mater Res Technol. 2025;36:217-235. https://doi.org/10.1016/j.jmrt.2025.03.131

16. Wang PQ, Chen DL, Ran Y, Yan YQ, She XW, Peng H, Jiang XQ. Electromagnetic pulse welding of Al/Cu dissimilar materials: Microstructure and tensile properties. Mater Sci Eng A. 2020;792:139842. https://doi.org/10.1016/j.msea.2020.139842

17. Sarvari M, Abdollah-zadeh A, Naffakh-Moosavy H, Rahimi A, Parsaeyan H. Investigation of Collision Surfaces and Weld Interface in Magnetic Pulse Welding of Dissimilar Al/Cu Sheets. J Manuf Process. 2019;45:356-367. https://doi.org/10.1016/j.jmapro.2019.07.012

18. Pourabbas M, Abdollah-Zadeh A, Sarvari M, Movassagh-Alanagh F, Pouranvari M. Role of collision angle during dissimilar Al/Cu magnetic pulse welding. Sci Technol Weld Join. 2020;25(7):549-555. https://doi.org/10.1080/13621718.2020.1768351

19. Deng F, Cao Q, Han X, Chen Q, Li L. Principle and realization of an electromagnetic pulse welding system with a dual-stage coil. Int J Appl Electromagn Mech. 2018;57(4):389-398. https://doi.org/10.3233/JAE-180053

20. Pabst C, Groche P. The Influence of Thermal and Mechanical Effects on the Bond Formation During Impact Welding. 2016. https://doi.org/10.17877/DE290R-16997

21. Christian P, Groche P. Identification of Process Parameters in Electromagnetic Pulse Welding and Their Utilisation to Expand the Process Window. Int J Mater Mech Manuf. 2018;6(1):69-73. https://doi.org/10.18178/IJMMM.2018.6.1.349

22. Kümper S, Schumacher E, Böhm S. Influence of the Ambient Pressure on the Weld Quality for Magnetic Pulse Welded Sheet Joints. 2018. http://dx.doi.org/10.17877/DE290R-18985

23. Bellmann J, Lueg-Althoff J, Niessen B, Böhme M, Schumacher E, Beyer E, Leyens C, Tekkaya AE, Groche P, Wagner MF-X, Böhm S. Particle Ejection by Jetting and Related Effects in Impact Welding Processes. Metals. 2020;10(8):1108. https://doi.org/10.3390/met10081108

24. Li X, Qian J, Han Y, Yang K, Wang Q, Sun B, Liu X, Zhang T. A comparative study on waveform prediction between SPH and S-ALE methods in impact welding. Ocean Eng. 2024;306. https://doi.org/10.1016/j.oceaneng.2024.118092

25. Han L, Li N, Chen Y, Wang J, Wang G, Zhang C, Li X. Interface microstructure morphology and formation evolution mechanism of Al-1060/Cu-T2 composites fabricated by explosive welding method. Compos Interfaces. 2021;29(5):465-485. https://doi.org/10.1080/09276440.2021.1971883

26. Wang S, Xu L, Sun T, Li G, Cui J. Effects of process parameters on mechanical performance and interfacial morphology of electromagnetic pulse welded joints between aluminum and galvanized steel. J Mater Res Technol. 2021;10:552-564. https://doi.org/10.1016/j.jmrt.2020.12.047

27. Geng H, Xia Z, Zhang X, Li G, Cui J. Microstructures and mechanical properties of the welded AA5182/HC340LA joint by magnetic pulse welding. Mater Charact. 2018;138:229-237. https://doi.org/10.1016/j.matchar.2018.02.018

28. Kore SD, Dhanesh P, Kulkarni SV, Date PP. Numerical modeling of electromagnetic welding. Int J Appl Electromagn Mech. 2010;32(1):1-19. https://doi.org/10.3233/JAE-2010-1062

29. Xu Z, Cui J, Yu H, Li C. Research on the impact velocity of magnetic impulse welding of pipe fitting. Mater Des. 2013;49:736-745. https://doi.org/10.1016/j.matdes.2012.12.059

30. Cui J, Wang S, Yuan W, Li G. Effects of Standoff Distance on Magnetic Pulse Welded Joints Between Aluminum and Steel Elements in Automobile Body. Automot Innov. 2020;3(3):231-241. https://doi.org/10.1007/s42154-020-00112-5

31. Raoelison RN, Racine D, Zhang Z, Buiron N, Marceau D, Rachik M. Magnetic pulse welding: Interface of Al/Cu joint and investigation of intermetallic formation effect on the weld features. J Manuf Process. 2014;16(4):427-434. https://doi.org/10.1016/j.jmapro.2014.05.002

32. Yao Y, Chen A, Wang F, Jiang H, Li G, Cui J. Mechanical properties and joining mechanisms of magnetic pulse welding joints of additively manufactured 316L and conventional AA5052 aluminum alloy. J Mater Res Technol. 2023;26:6146-6161. https://doi.org/10.1016/j.jmrt.2023.09.008

Figure captions

Fig 1 EMPW platform for different environmental pressures: (a) electromagnetic pulse workpiece; (b)data detection part

Fig 2 EMPW process of Al-Cu plates in different environment pressures: (a) relative position and geometry of plates; (b) vacuum energy storage and discharge; (c) dynamic response of the flyer plate; (d) metallurgical bonding

Fig 3 Weld inspection: (a) weld zone; (b) strip test method; (c) ultrasound testing method

Fig 4 Macroscopic deformation processes of Al and Cu plates colliding(a) 0 μs；(b) 16.5 μs；(c) 19.1 μs；(d) 21 μs

Fig 5 PDV and simulated velocity-displacement curves

Fig 6 S-ALE simulation modeling process:(a) oblique collision modeling; (b) meshing; (c) background meshing

Fig 7 Welding interface comparison image:(a) S-ALE simulation; (b) SEM microscopic observation

Fig 8 Load-displacement curves and failure forms of welded specimens with different process parameters

Fig 9 Mechanical properties under different vacuum environment pressures: (a) load-displacement curves; (b) peak tensile loads

Fig 10 Discharge energy - environment pressure welding window

Fig 11 NDT of welds in different environment pressures: (a) inspection area; (b) typical weld morphology; (c) NDT images

Fig 12 Analysis of weld morphology in different environment pressures: (a) segmentation and extraction of images; (b) weld outer width and weld outer length; (c) weld internal width and weld area

Fig 13 EMPW welding process flyer plate morphology change schematic diagram

Fig 14 Velocity-displacement curves of flyer plates under different environment pressures

Fig 15 Simulation results of velocity during EMPW process at 101 kPa:(a)1.5 μs；(b) 3 μs；(c) 4.5 μs

Fig 16 Simulation results of velocity during EMPW process at 20 kPa:(a)1.5 μs；(b) 3 μs；(c) 4.5 μs

Fig 17 Simulation results of microscopic material distribution at the interface of Al-Cu welded joints under different environment pressures: (a) 101 kPa; (b) 20 kPa

Fig 18 S-ALE simulation results of Al-Cu welding process at 101 kPa:1.5 μs; (b) 3 μs; (c) 4.5 μs; (d) 6 μs

Fig 19 S-ALE simulation results of Al-Cu welding process at 20 kPa:(a) 1 μs; (b) 2 μs; (c) 3.8 μs; (d) 6 μs

Fig 20 EMPW interface structure in two different environment pressures: (a) 101 kPa environmental pressure; (b) 20 kPa environmental pressure

Fig 21 Schematic diagram of the evolution of the dynamic behavior of the flyer plate in EMPW: (a) Stage 1; (b) Stage 2; (c) Stage 3; (d) Stage 4

Fig 22 SEM and EDS images of the weld interface at 101 kPa: (a) typical morphology of weld interface; (b) elemental distribution; (c) and (d) show the EDS scans of line 1 and line 2, respectively

Fig 23 SEM and EDS images of the weld interface at 20 kPa: (a) typical morphology of weld interface; (b) elemental distribution; (c) and (d) show the EDS scans of line 1 and line 2, respectively

Table captions

Table 1 Mechanical properties and chemical compositions of two materials

Table 2 Air constitutive model and its equation of state parameters at different environment pressures

Table 3 Peak tensile loads and failure forms of repetitive specimens

Table 4 Failure forms, peak loads and weld morphology of welded joints at different environment pressures

Table 5 Flyer plate velocity at different environmental pressures